Atmospheric
Chemistry
and Physics

Variations of cloud condensation nuclei (CCN) and aerosol activity during fog–haze episode: a case study from Shanghai

C. Leng[1], Q. Zhang[1], D. Zhang[1], C. Xu[1], T. Cheng[1,2], R. Zhang[3], J. Tao[4], J. Chen[1,2], S. Zha[1], Y. Zhang[1], X. Li[1], L. Kong[1], and W. Gao[5]

[1]Shanghai Key Laboratory of Atmospheric Particle Pollution and Prevention (LAP3),
Department of environmental science and engineering, Fudan University, Shanghai 200433, China
[2]Fudan-Tyndall Centre, Fudan University, Shanghai 200433, China
[3]Key Laboratory of Region Climate-Environment Research for Temperate East Asia,
Institute of Atmospheric Physics, Chinese Academy of Sciences, Beijing 100029, China
[4]South China Institute of Environmental Sciences, Ministry of Environmental Protection,
Guangzhou 510655, China
[5]Shanghai Meteorological Bureau, Shanghai 200030, China

Correspondence to: T. Cheng (ttcheng@fudan.edu.cn) and J. Chen (jmchen@fudan.edu.cn)

Abstract. Measurements of cloud condensation nuclei (CCN), condensation nuclei (CN) and aerosol chemical composition were performed simultaneously at an urban site in Shanghai from 6 to 9 November 2010. The variations of CCN number concentration (N_{CCN}) and aerosol activity (activated aerosol fraction, N_{CCN}/N_{CN}) were examined during a fog–haze co-occurring event. Anthropogenic pollutants emitted from vehicles and unfavorable meteorological conditions such as low planetary boundary layer (PBL) height exerted a great influence on $PM_{2.5}$ and black carbon (BC) loadings. N_{CCN} at 0.2 % supersaturation (SS) mostly fell in the range of 994 to 6268 cm^{-3}, and the corresponding N_{CCN}/N_{CN} varied between 0.09 and 0.57. N_{CCN} and N_{CCN}/N_{CN} usually were usually higher in the hazy case due to increased aerosol concentration in the accumulation mode (100–500 nm), and lower in the foggy–hazy and clear cases. The BC mass concentration posed a strong positive effect on N_{CCN} in the foggy–hazy and hazy cases, whereas it poorly correlated with N_{CCN} in the clear case. N_{CCN}/N_{CN} was weakly related with BC in both foggy–hazy and hazy cases. By using a simplified particle hygroscopicity (κ), the calculated critical dry size (CDS) of activated aerosol did not exceed 130 nm at 0.2 % SS in spite of diverse aerosol chemical compositions. The predicted N_{CCN} at 0.2 % SS was very successful compared with the observed N_{CCN} in clear case ($R^2 = 0.96$) and foggy–hazy/hazy cases ($R^2 = 0.91$). In addition, their corresponding ratios of predicted to observed N_{CCN} were on average 0.95 and 0.92, respectively. More organic matter is possibly responsible for this closure difference between foggy–hazy/hazy and clear cases. These results reveal that the particulate pollutant burden exerts a significant impact on N_{CCN}, especially N_{CCN}/N_{CN} promotes effectively during the polluted periods.

1 Introduction

Cloud condensation nuclei (CCN), which constitutes an important fraction of atmospheric aerosol, can influence the microphysical and radiative properties and lifetime of cloud indirectly and consequently impact the hydrological cycle (IPCC, 2013). Elevated CCN loadings (N_{CCN}) tend to reduce cloud droplet size and then suppress precipitation in shallow and short-lived clouds (Lohmann and Feichter, 2005), in addition to which they can promote great convective overturning and enhance precipitation in deep convective clouds (Rosenfeld et al., 2008). Numerous aerosol properties, including particle size distribution, chemical composition and mixing state, are closely linked with the ability of particles to take up water vapor, i.e., the ability to act as CCN (Baum-

gardner et al., 2003; Kuwata and Kondo, 2008; Cubison et al., 2008). To date, the current assessment of aerosol indirect effects induced by increasing anthropogenic aerosols remains poorly understood, and this brings a big uncertainty in fully picturing climate change (Andreae et al., 2005; IPCC, 2013).

Owing to advanced instrument development, the aerosol-cloud interaction and its impact on climate have attracted increasing attention in the last decades. Many ground-based measurements on CCN have been performed in diverse environments, describing a global map of CCN distribution in the surface atmosphere (Baumgardner et al., 2003; Yum et al., 2004, 2005; Reade et al., 2006; Juranyi et al., 2010; Leng et al., 2013). In urban environments, the new particle formation and growth, and haze pollution were observed recently as having a significant impact on N_{CCN} (Ritesh et al., 2007; Kuang et al., 2009). In recent years, CCN studies have raised the relative importance of several influence factors controlling aerosol CCN activity, of which size has been announced as the major factor in determining the CCN activation of aerosol particles (Dusek et al., 2006; Anttila and Kerminen, 2007; Hudson, 2007; Quinn et al., 2008; Jimenez et al., 2009; Leng et al., 2013). However, how chemical composition especially organic compounds to link with aerosol activity and then CCN has not been fully understood. In fact, up to 90 % of the aerosol mass concentration consists of carbonaceous substances, and among them 10–70 % is water-soluble (Moffet et al., 2008; Stone et al., 2008). Particularly, various externally or internally mixed particulate components comprised in urban air mass can significantly affect the CCN-sized spectra of atmospheric particles (Svenningsson et al., 2006; Reade et al., 2006; Kuwata et al., 2007). This has posed a major challenge to study aerosol composition and predict CCN activity (Hagler et al., 2007; Hings et al., 2008; Henning et al., 2010).

Due to rapid industrialization in Asia for decades, anthropogenic particles and relevant precursor emissions have increased significantly, and numerous studies have indicated that the increasing anthropogenic aerosol loading has significantly changed cloud microphysical and radiative properties (Streets et al., 2000, 2008; Shao et al., 2006; Wang et al., 2006; Qian et al., 2006; Rosenfeld et al., 2007; Matsui et al., 2010; Zhang et al., 2013). In China, studies on CCN have been done widely such as at polluted sites located in Yufa (Wiedensohler et al., 2009), Beijing (Yue et al., 2011), Shouxian (Liu et al., 2011) and Shanghai (Leng et al., 2013), and suburban sites in Guangzhou (Rose et al., 2010, 2011) and Wuqing (Deng et al., 2011). To our knowledge, little attention has been paid on the impacts of fog or haze on CCN and activated aerosol particles. The increases of haze occurrences are evident in the eastern and southwestern cities in China (Che et al., 2009). Shanghai is a huge metropolis in China, and the occurrence intensity of foggy and hazy days on annual time scale has been increasing gradually especially in winter (Tie and Cao, 2009), which is deeply affected by

fine particle pollution enhancement and possibly linked with particle hygroscopicity (Ye et al., 2011).

This study presents continuous measurements of CCN and aerosol during a fog–haze episode from 6 to 9 November 2010 in Shanghai. The aim is to provide insights on CCN and aerosol activity variations under fog–haze co-occurring conditions. The instrumentation and data used in the study are described in Sect. 2. The aerosol physical and chemical properties are introduced in Sect. 3. Section 4 presents the evolution of CCN and aerosol activity. The relationship between aerosol and CCN is discussed in Sect. 5. Conclusions from the study are given in Sect. 6.

2   Methods

2.1   Observational site

The instruments for CCN and aerosol measurements have been mounted roughly 20 m above ground on the roof of a building in the campus of Fudan University in Shanghai (31°18′ N, 121°29′ E) since October 2010. The site is surrounded by populated residential and commercial areas, as well as urban streets. The East China Sea is roughly 40 km east of the site, and the prevailing wind directions are southeasterly in summer and northeasterly in winter. Local time (LT) hereafter employed in this study is 8 h ahead of UTC.

2.2   Measurements and methodology

The CCN number concentration (N_{CCN}) was measured using a continuous flow and single column CCN counter (model CCN-100, Droplet Measurement Technologies, USA), in which an optical particle counter (OPC, 0.75–10 μm) is employed to detect activated cloud droplets (Roberts and Nenes, 2005; Lance et al., 2006). The instrument was housed in an air-conditioned weather-proof container with temperature maintaining at 20 °C. The ambient aerosol airflow passed through a dryer (active carbon) to lower relative humidity below 30 % before entering the instrument (Leng et al., 2013). The CCN counter was calibrated using ammonium sulfate before the study, as did calibrations for temperature gradient, flow, pressure and OPC to maintain stable supersaturation (SS) according to the Droplet Measurement Technology (DMT) operation manual. In order to ensure accurately counting, zero checks were performed before and after the campaign and regularly every 2 months. The effective water vapor (SS) changed alternately at 0.2 % interval within 0.2–1.0 %. In real atmosphere, SS varies from slightly less than 0.1 % in polluted conditions to over 1.0 % in clean-air stratus cloud (Hudson and Noble, 2014). The selection of SS 0.2 % in the present study would benefit to the measurements in the urban environment for further analysis. Although the CCN counter can operate well under conditions of particles only in the range of a few thousand per cubic centimeter, and corrections are needed for larger concentrations

($> 5000 \, \text{cm}^{-3}$) (Lathem and Nenes., 2011), we still used the measured N_{CCN} directly at 0.2 % SS in this study since it seldom reached the upper limit.

A high-resolution wide-range particle spectrometer (WPS-1000 XP, MSP) was employed to observe particle size distributions in the size range of 10 nm-10 µm. The principles of the instrument, which have been introduced in detail by Gao et al. (2009), combine laser light scattering (LPS), condensation particle counting (CPC), and differential mobility analysis (DMA). The DMA and CPC can effectively measure aerosol particles distributed in the size range of 10–500 nm in up to 96 channels. The LPS scan the size range of 350–10 000 nm in 24 additional channels. In the present study 60 channels in DMA and 24 channels in LPS for the sample mode were chosen and 3 min were needed to scan the entire size range completely, as it took 2 s for scanning each channel. DMA was calibrated with National Institute of Standards and Technology (NIST) Standard Reference Materials (SRM) 1691 and SRM 1963 Polystyrene Latex (PSL) spheres (mean diameter of 0.269 and 0.1007 µm, respectively) to maintain DMA transfer function properly and accurate particle sizing traceable to NIST. Four NIST traceable sizes of PSL (i.e., 0.701, 1.36, 1.6 and 4.0 µm) were used to calculate LPS. The calibration and operating methodology of WPS has been described elsewhere (Zhang et al., 2010). In addition, we have compared the aerosol size spectra measured by WPS with those measured in parallel by a calibrated scanning mobility particle sizer (SMPS, TSI 3080) with higher accuracy in the size range of 20–800 nm, including size-resolved particle concentrations and peak sizes, and a strong correlation between them was derived with correlation coefficient $R^2 > 0.95$ (Leng et al., 2013). The result confirms the reliability of WPS measurements for successfully characterizing the number concentration and size distribution of condensation nuclei (CN).

Planetary boundary layer (PBL) height and aerosol vertical extinction profile were measured using a set of micro pulse lidar (MPL) system (MPL-4B-532) with pulse energy 6–10 µJ and pulse repetition frequency 2500 Hz. The MPL is an eye safe, compact and autonomous instrument, and an effective tool used widely in the world to provide available high spatial (30 m) and temporal resolution (30 s) information of aerosol vertical distributions (Menut et al. 1999; Cohn and Angevine, 2000; Brooks, 2003). The range of lidar is roughly 30 km at night and 10 km during the daytime. The description of the retrieval of aerosol parameters by the MPL will be only briefly summarized here as it has been given by He et al. (2006). The vertical profile of the aerosol extinction coefficient is determined by a near end approach in solving the lidar equation (Fernald, 1984). The PBL height is determined by the MPL lidar at the altitude where a sudden decrease of scattering coefficient occurs (Boers and Eloranta, 1986). The overlap problem must be solved because it can lead to an underestimation of aerosol backscatter and extinction coefficients in the lowest altitudes having the majority of aerosols

(He et al., 2006a). Outlined by Campbell et al. (2002), overlap is typically solved experimentally. The system is set to point horizontally to an averaged data sample with no obscuration, such as the late afternoon, when the atmosphere is well mixed and the aerosol loading is low. The backscattering over the target layer is roughly assumed constant. The similar calibration performed in 2009 showed the full overlap of about 4 km and data are needed to be corrected by the overlap correction function. Welton et al. (2002) fully discussed the uncertainties caused by the overlap correction and He et al. (2006) estimated it to be less than 10 %.

An online Aethalometer (AE-31, Magee Scientific Co., Berkeley, California, USA) was employed to measure black carbon (BC) at a 5 min time resolution. The instrument was operated at an airflow rate of $5 \, \text{L} \, \text{min}^{-1}$. Based on the strong absorptivity of BC to light at near infrared wavelengths (Hansen et al., 1984; Weingartner et al., 2003), BC concentration is determined using the measured light attenuation at 880 nm and the appropriate value of specific attenuation cross section proportional to BC mass (Petzold et al., 1997). The attenuation can be obtained by calculating the difference between light transmission through the particle-laden sample spot and the particle-free reference spot in the filter (Cheng et al., 2006; Dumka et al., 2010). The operation, calibration and maintenance of AE-31 have been described in detail by Cheng et al. (2010).

An online analyzer for Monitoring Aerosols and Gases (MARGA, ADI 2080, Netherlands) was employed to measure the concentration of major inorganic water-soluble ions (e.g., Na+, K^+, Mg^+, Ca^+, SO_4^{2-}, Cl^-, NO_3^- and NH_4^+) in ambient aerosol particles at 1 hour time resolution. An air pump controlled by a mass flow controller (MFC) draws ambient air with airflow of $1 \, \text{m}^3 \, \text{hr}^{-1}$ into the sample box. An internal calibration method by using bromide for the anion chromatograph and lithium for the cation chromatograph was operated over the entire measurement period to ensure this instrument to identify and measure ion species successfully. Instructions for the methods of sampling, operation and internal calibration have been described in detail elsewhere (Du et al., 2011). Moreover, the mass concentrations of particulate matter (PM) with aerodynamic diameter less than 2.5 µm ($PM_{2.5}$), meteorological factors and atmospheric visibility were measured by a continuous PM ambient monitor (FH62C14, Thermo), an automatic weather monitoring system (HydroMet[TM], Vaisala) and a automatic visibility monitor at 5 min time resolution, respectively.

2.3 Air mass backward trajectory

The HYSPLIT-4 model developed by the Air Resources Laboratory (ARL) of the National Oceanic and Atmospheric Administration (NOAA), USA (Draxler et al., 2003), was employed to compute 24 h air mass backward trajectories ending at 500 m height (AGL) and starting at 00:00 LT and 12:00 LT for each day. By doing so, we can identify aerosols
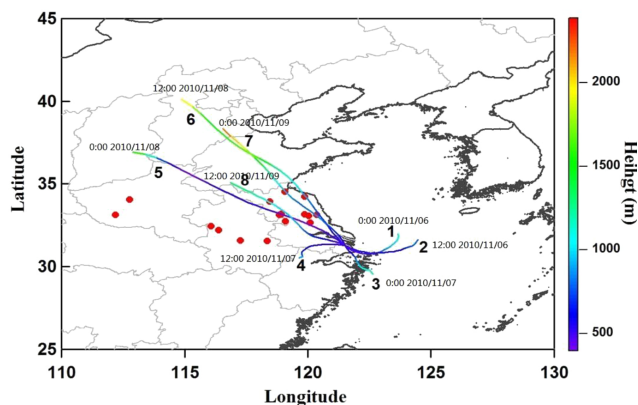
Figure 1. Agricultural fire scattering areas and air mass transport pathways across these regions. All red spots represent biomass burning sites on 7 November measured from MODIS satellite. Starting time (LT) is labeled in the figure.

Figure 2. Temporal variations of temperature, wind speed and direction, RH, pressure and atmospheric visibility, the foggy–hazy case is marked in red open boxes and the hazy case in black.

from different source regions and analyze their effects on aerosol activity to compile a full view of the relation between fog–haze event and N_{CCN}. According to these calculated trajectories plotted in Fig. 1, aerosol was classified into two categories: (1) maritime aerosol transported by air masses from marine areas on 6 November 2010 carrying dominant oceanic particles and (2) continental aerosol in air mass traveling a long distance over inland areas on 7, 8, and 9 November 2010 and carrying more anthropogenic particles (e.g., BC). Exactly speaking, the maritime air mass originated from the East China Sea, slowly traveled northwesterly across the Hangzhou Bay and finally arrived in Shanghai on 6 November. Then the air mass changed its path southeasterly at around 12:00 a.m. on 7 November, and traveled from northern inland areas and across the North China Plain (NCP) and the eastern region of China. The continental sources contained increasing industrial and agricultural emissions (e.g., biomass burning) due to long-term rapid economy growth and large population in the last few decades. We hope to better understand the impact of aerosols with or with less anthropogenic particulate pollutants on CCN in this study by comparing these two categories.

3 Results

3.1 Overview of the fog–haze event

Haze is traditionally defined as an atmospheric phenomenon that the sky clarity is obscured by dust, smoke and other dry particles, and atmospheric visibility and relative humidity (RH) are usually less than 10 km and 80 % over one haze episode (Fu et al., 2008). The high frequency of haze or hazy days is observed in winter, especially in the urban environments of northern China (Sun et al., 2006). During the haze event, the enhancement of particulate pollutants may greatly
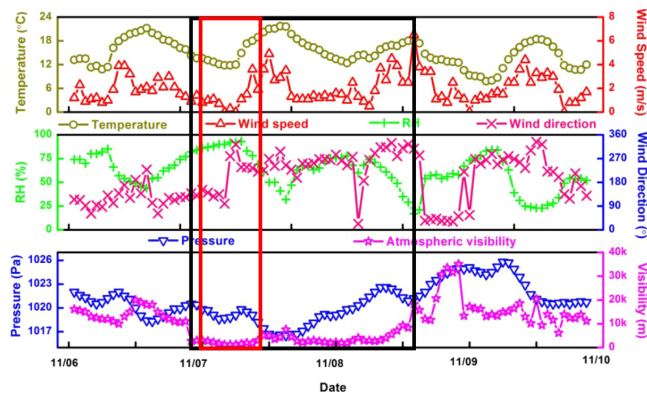
affect aerosol activity and N_{CCN}. The study performed in the Indo–Gangetic plain shows that winter haze exerts a significant impact on the fog and low-cloud formation (Gautam et al., 2007).

Fog can be viewed as a lower-atmospheric near-surface cloud, and plays an important role in processing aerosol particles and trace gases (Gultepe et al., 2007; Biswas et al., 2008). On one hand, physically similar to cloud droplet, fog droplet also forms by water vapor condensing on dry aerosol particle under supersaturated conditions. On the other hand, generally formed in the shallow boundary layer containing local emissions, urban fog traps more pollutants than cloud at high altitudes (Fisak et al., 2002; Herckes et al., 2007). A fog or foggy case is defined as a weather with patterns of low visibility (< 10 km) and high (> 90 %) relative humidity (RH). When 80 % < RH < 90 %, the weather was referred to as a complex of haze and fog co-occurring (e.g., foggy–hazy) in the present study. Figures 2 and 3 show a 4 day time series of pressure, atmospheric visibility, RH, temperature, wind speed and direction, and PBL height from 6 to 9 November 2010. In fact, since RH seldom reached up to 90 %; thus the period focused in the present study was characterized by both hazy and foggy–hazy cases. The haze pollution lasting at least 4 hours has been identified as one haze event by an earlier study in Shanghai, where authors paid attention to the formation of haze pollution (Du et al., 2011).

As shown in Figs. 2–8, the 4 day period was classified into three parts: a hazy episode (marked in black open boxes) from 22:00 to 23:00 LT on 6 Noveber and 10:00 LT on 7 November to 13:00 LT on 8 November, a foggy–hazy episode (marked in red open boxes) from 23:00 LT on 6 November to 10:00 LT on 7 November, and the rest for clear case. Statistics for meteorological conditions is listed in Table 1 where the extinction profiles are averaged for a certain altitude of 500 m. During the hazy and foggy–hazy cases, the average atmospheric visibility was about 4.44 km and 2.33 km, respectively, much lower than 15.4 km in the clear case. The

Table 1. Statistics of meteorological parameters in different weather conditions.

	Clear day	foggy–hazy day	hazy day	All
Temperature (°C)	14.4	14.6	16.6	15.0
Wind direction (deg)	157.2	191.4	260.6	191.3
Wind speed (m s^{-1})	1.9	1.3	2.3	1.9
Pressure (hPa)	1021.9	1019.2	1019.5	1020.8
RH (%)	58.1	84.9	58.3	62.0
Visibility (km)	15.4	2.3	4.4	10.4
PBL (km)	0.42	0.71	0.78	0.55
Extinction coefficient	0.32	0.27	0.76	0.62
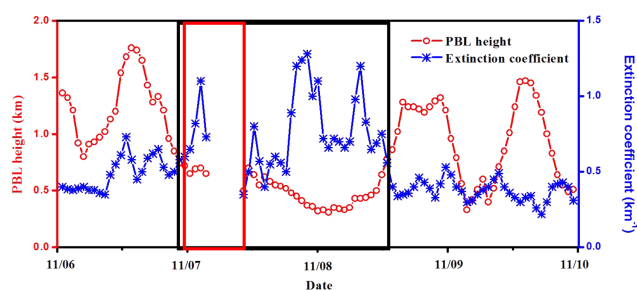
Figure 3. Temporal variations of PBL and vertical extinction coefficient (500 m) measured by MPL lidar. Data from 05:00–09:00 on 7th are labeled as invalid and not shown. The foggy–hazy case is marked in red open boxes and the hazy case in black.
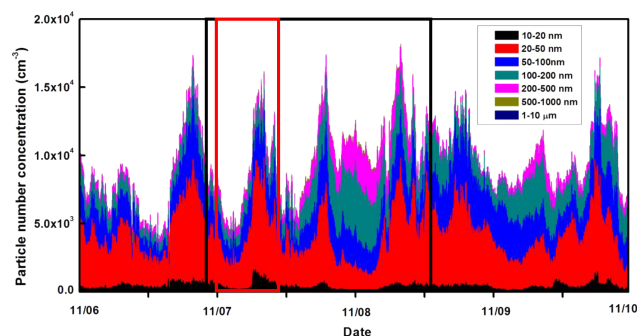
Figure 4. Hourly mean particle number concentrations of different sub-size bins, the foggy–hazy case is marked in red open boxes and hazy case in black.

winds from the east and the south brought clean maritime aerosol during the clear case, however, the winds from the north and the west brought polluted anthropogenic aerosol during the hazy and foggy–hazy cases. The particulate and gaseous matters, including pollutants (e.g., BC) emitted from agricultural biomass burning were transported along the air mass pathways (Fig. 1), led to a significant enhancement of aerosol extinction coefficient from hourly averages of 0.5 to 1.2 km^{-1} (Fig. 3). In addition, the PBL height downed to below 500 m and further suppressed the dilution of pollutants.
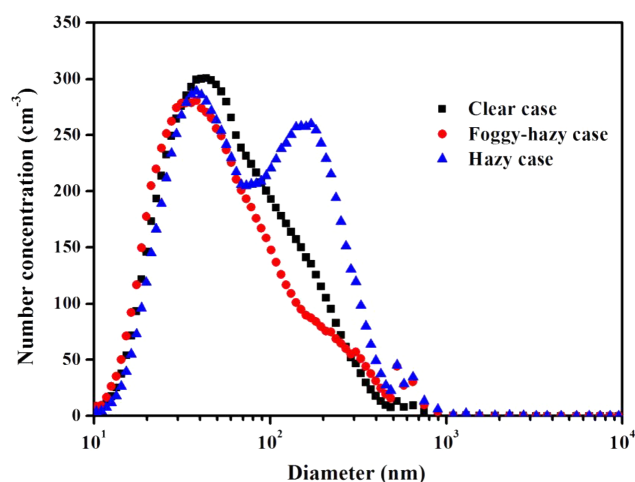
Figure 5. Average size distributions (10 nm–10 μm) for all the hazy, foggy–hazy, and clear cases.

3.2 Physical and chemical properties of aerosol

In order to visually identify aerosol evolution, particles in the size range of 10 nm to 10 μm were categorized into 7 sub-size bins: 10–20 nm (nucleation mode), 20–50 nm and 50–100 nm (Aitken mode), 100–200 nm, 200–500 nm and 0.5–1 μm (accumulation mode), and 1–10 μm (coarse mode) (Fig. 4). A similar classification was applied to the measurements at the same site by Zhang et al. (2010). In this study, the integrated-particle size-resolved number concentrations N_{CN}) exhibited a regular diurnal cycle, with two peaks (9000–16 000 cm^{-3}) almost within the traffic rush hours. The mean N_{CN} exhibited no obvious difference between the foggy–hazy (8367 cm^{-3}) and clear (8956 cm^{-3}) cases, but it showed a higher value (10 500 cm^{-3}) in the hazy cases, revealing a larger loading of particulate pollutants.

In general, 20–100 nm (Aitken mode) particles dominated the particle number size distribution, probably due to local traffic emissions and meteorological conditions (Ferin e al., 1990). The temporal variation trend of Aitken mode was similar to N_{CN}. It was interesting that the particles of 100–500 nm (accumulation mode) dominated in N_{CN} in the
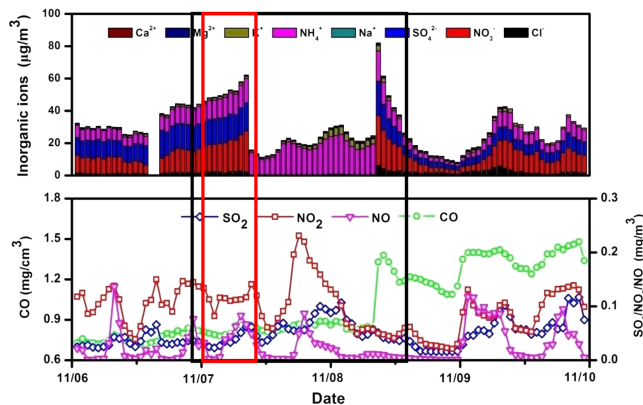
Figure 6. Temporal variations of particle water soluble ion composition and trace gases, the foggy–hazy case is marked in red open boxes and hazy case in black.

Figure 7. Temporal variations of N_{CN}, N_{CCN} at 0.2 % SS, BC, $PM_{2.5}$ and N_{CCN}/N_{CN}, the foggy–hazy case is marked in red open boxes and hazy case in black

Figure 8. Temporal variations of $CN_{100\,nm-10\,\mu m}$, $CN_{80\,nm-10\,\mu m}$, $CCN/CN_{100\,nm-10\,\mu m}$ at 0.2 % SS and $CCN/CN_{80\,nm-10\,\mu m}$ at 0.2 % SS, the foggy–hazy case is marked in red open boxes and hazy case in black.

hazy case with peak concentrations higher than $7500\,cm^{-3}$, almost twice as much as the clear case ($4000\,cm^{-3}$). However, the foggy–hazy case is comparable to the clear case, showing a mostly unchanged evolution of the fractions of individual size bin to total particles and N_{CN}. In addition, Fig. 5 shows the average size distributions ($10\,nm-10\,\mu m$) for all the three cases. It is very visible that it contains relatively more large-sized (e.g., 100 nm) aerosol particles in the aerosol population during the hazy case than that during the clear and foggy–hazy cases. Especially aerosol particles larger than 200 nm (a typical CCN size at SS 0.2 %) were significantly enhanced.

Figure 6 shows the temporal variations of eight major inorganic water soluble ions in aerosol particles and four gaseous pollutants sampled during this study period. Measurements for SO_4^{2-}, Cl^- and NO_3^- were unavailable from 10:00 LT on 7 November to 08:00 LT on 8 November. Substantially, the average concentration of aerosol total water soluble ions (TWSI) in the hazy case ($54.5\,\mu g\,m^{-3}$) was comparable to the foggy–hazy case ($50.4\,\mu g\,m^{-3}$), and roughly 2 times that of the clear case ($26.2\,\mu g\,m^{-3}$). For the percentage of individual ions in TWSI, NH_4^+ and K^+ were relatively higher by a factor of 1.8 in the hazy and foggy–hazy cases than in the clear case. Despite the lack of SO_4^{2-} and NO_3^- partly during the hazy case, we can still conjecture their promotion on the basis of their gaseous precursor evolution of SO_2 and NO_2.

Gaseous pollutants are released into the atmosphere from natural and anthropogenic emissions. Among them, SO_2 is known as one of the most important gaseous pollutants and a precursor responsible for acid rain. Also, it can participate in the formation of new particles through converting into gaseous H_2SO_4, which is the most common nucleation species due to its low vapor pressure at typical atmospheric temperature (Zhang et al., 2006b; Urone et al., 1968). Secondary aerosols produced from the formation of new particles contribute more to the global burden of aerosol num-
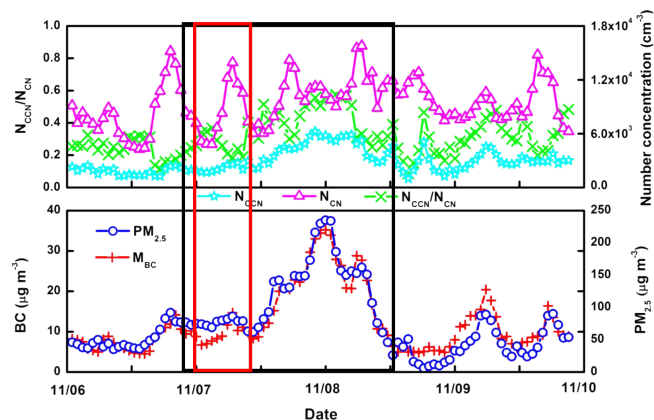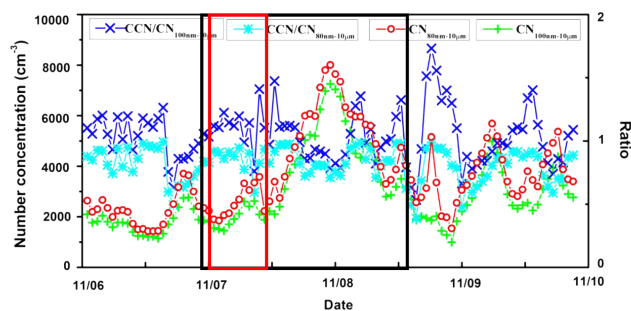
ber than primary aerosols and are important sources of CCN (Merikanto et al., 2009; Yu et al., 2008). Recent studies have shown the enhanced solubility of SO_2 due to its reaction in fog droplets during a severe fog measured in the North China Plain, and this finding has provided important support for better understanding of the acidity in clouds (Zhang et al., 2013). NO_2 mainly comes from vehicle traffic emissions in urban areas (Wang et al., 2006). Nitrogen oxides (NO, NO_2, N_2O_5) undergo heterogeneous reactions with aerosol particles (e.g., sea salt or dust) during they are transported in the atmosphere (Elizabeth et al., 2006). Thus, high gaseous pollutant content can result in larger CN loadings and subsequently more CCN particles in the atmosphere. On the whole, the loading of these precursor gases in the foggy–hazy and hazy cases exceeded that in the clear case, specifically NO_2 by a factor of 2 and SO_2 by a factor of 1.5. Moreover, SO_2 and NO_2 concentrations reached their peaks around 00:00 LT on 8 November corresponding to the highest levels of CCN and aerosol activity, implying their potential effects on CCN production, which will be discussed in the next section.

Table 2. Statistics of CCN, CN, CCN/CN and BC in different weather conditions.

	Clear day	Foggy–hazy day	Hazy day	All
CCN range (cm^{-3})	994–5096	1677–2947	2088–6268	994–6268
CCN average (cm^{-3})	2432	2377	4362	2929
CN range (cm^{-3})	4270–15 168	4815–13 922	6033–15 771	4270–15 771
CN average (cm^{-3})	8956	8367	10 500	9344
CCN/CN range	0.09–0.48	0.18–0.40	0.25–0.57	0.09–0.57
CCN/CN average	0.28	0.29	0.41	0.32
BC range ($\mu g\,m^{-3}$)	4.51–20.40	6.7–14.7	8.3–35.2	4.51–35.20
BC average ($\mu g\,m^{-3}$)	8.57	9.58	21.26	12.24

3.3 CCN Concentration and aerosol activity

3.3.1 CCN and Aerosol Activity

Figure 7 presents the temporal variations of N_{CCN} and activated aerosol fraction (N_{CCN}/N_{CN}) at SS 0.2 %, N_{CN}, and BC during the campaign. Totally, N_{CN} fell in the range of 4270–15 771 cm^{-3} and averaged at 9344 cm^{-3}, and N_{CCN} varied between 994 cm^{-3} and 6268 cm^{-3} and averaged at 2929 cm^{-3}. High N_{CCN}/N_{CN} (0.41) and N_{CCN} (4362 cm^{-3}) were observed during the hazy case, followed by the foggy–hazy (0.29, 2377 cm^{-3}) and clear (0.28, 2432 cm^{-3}) cases (Table 2). The temporal variation of N_{CCN}/N_{CN} and N_{CCN} was closely related with aerosol particle size spectra and chemical composition such as accumulation mode (100–500 nm) and water soluble ion content (Figs. 4 and 6). Figure 8 gives the temporal variations of number concentrations of larger aerosol particles (e.g., particles larger than 80 nm and 100 nm) and their corresponding ratios with N_{CCN} at SS 0.2 %. The larger aerosol particles showed significant increase during the hazy case and varied strongly correlated with N_{CCN}. More fractions of particles larger than 80 nm were activated into CCN during the hazy case (86 %) and foggy–hazy case (84 %) than that during the clear case (76 %).

Although in different SS conditions, N_{CCN} was measured at other urban or urban-like environments such as the west coast of Tasmania (32 cm^{-3}) and the west coast of Korea (5292 cm^{-3}) at SS 1.0 % (Yum et al., 2004, 2005), and Mexico city (3000 cm^{-3}), Ireland (208–346 cm^{-3}) and Vienna (820 cm^{-3}) at SS 0.5 % (Baumgardner et al., 2003; Reade et al., 2006; Burkart et al., 2011). An even larger N_{CCN} (6000 cm^{-3}) was measured at SS 0.17 % in Beijing (Deng et al., 2011). The average N_{CCN}/N_{CN} of this study (0.32) was higher than that measured in Vienna (0.13 at SS 0.5 %, CN 13-929 nm) and Finland (0.1–0.3 at SS 0.2 %, CN 3–1000 nm). The increased N_{CCN}/N_{CN} was derived at larger SS in urban environments such as Shanghai (0.47 at SS 0.8 %, CN 10–10 000 nm) and Korea (0.64 at SS 1.0 %, CN 10–500 nm) (Yum et al., 2005; Burkart et al., 2011; Sihto et al., 2011; Leng et al., 2013).

As expected, N_{CN} behaved in diurnal cycle with an apparent pattern of bi-modal distribution, and N_{CCN} showed a similar temporal variation (Fig. 7). N_{CN} and BC usually peaked, and reached their highest values of 15 000 cm^{-3} and 35 $\mu g\,m^{-3}$ during the rush hours (i.e., 07:00–09:00 and 16:00–19:00 LT), indicating that the anthropogenic pollutants emitted from vehicles contributes to a large part of CN and BC loadings. In addition, the favorable meteorological conditions such as low wind speed, temperature and planetary boundary layer (PBL) height also posed a great influence on $PM_{2.5}$ and BC loadings (Fig. 3). For example, the low wind speed (about 2 $m\,s^{-1}$) and PBL height (around 0.5 km) favored the mass accumulations of $PM_{2.5}$ and BC reaching their maximums of 242 and 35 $\mu g\,m^{-1}$ at 00:00 on 8 November. The later disappearance of the haze pollution was mostly due to the wind speed increasing to 6 $m\,s^{-1}$ and the PBL height rising to 1.4 km (Fig. 2). Temperature is known as a large factor influencing PBL height and thereby indirectly impacts $PM_{2.5}$ and BC. In addition, the wind was frequently from the northwest direction and brought a large amount of anthropogenic particles (e.g., BC) to Shanghai during the foggy–hazy/hazy cases, while it blew easterly or northeasterly (marine area) before and after the polluted cases (Figs. 1, 2 and 7).

In a broad view, N_{CCN} showed a sharp increase starting at 00:00 LT on 8 November, and rose from 994 cm^{-3} to 6268 cm^{-3} within less than 10 hours. Similar to N_{CCN}, BC also rose from 10 $\mu g\,m^{-3}$ to 35 $\mu g\,m^{-3}$ during the same period. N_{CN} was consistent with N_{CCN}, and they varied almost synchronously. However, N_{CCN}/N_{CN} changed in one step mostly opposite to N_{CCN} and N_{CN} (Fig. 7). The possible reason for this contradictory tendency of N_{CN} enhancement vs. N_{CCN}/N_{CN} reduction is that the unactivated nanoparticles, which burst partly from primary emissions of vehicles and/or partly from secondary particles due to the chemical reactions of atmospheric gaseous precursors (Fig. 5) (Du et al., 2011), contributes relatively larger to N_{CN} other than N_{CCN}.

Table 3. Effective hygroscopicity parameters (κ_i), and densities of the three category compositions in fine particles (Yue et al., 2011).

Species	Data source	κ_i	Density (g cm^{-3})
Sulfate and Nitrate	$SO_4^{2-} + NO_3^- + NH_4^+$	0.6	1.7
Sodium chloride and marine aerosols	$Na^+ + Cl^-$	1.0	2.2
Insoluble compounds	BC	0	1.0
	others	0	2.0
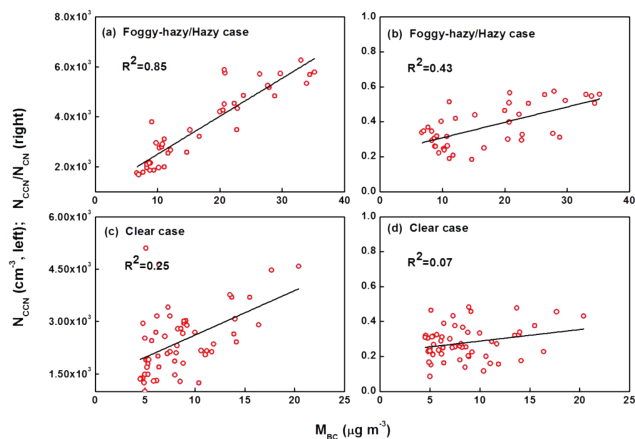
Figure 9. Correlations of BC mass concentration (M_{BC}) to N$_{CCN}$ and N$_{CCN}$/N$_{CN}$ (0.2 % SS).
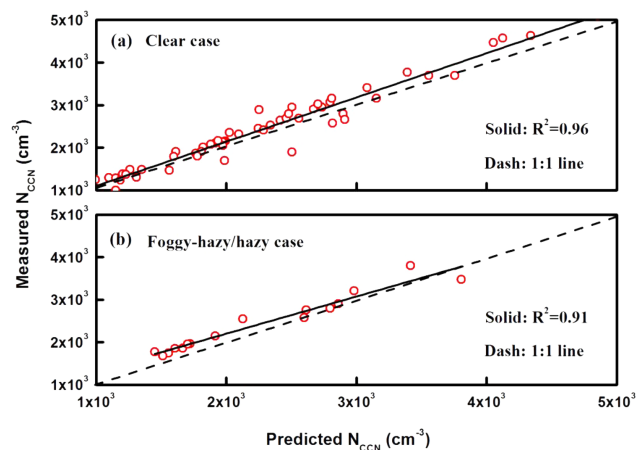
Figure 11. Correlations of observed and predicted N$_{CCN}$ (0.2 % SS) in the clear **(a)** and foggy–hazy/hazy **(b)** cases
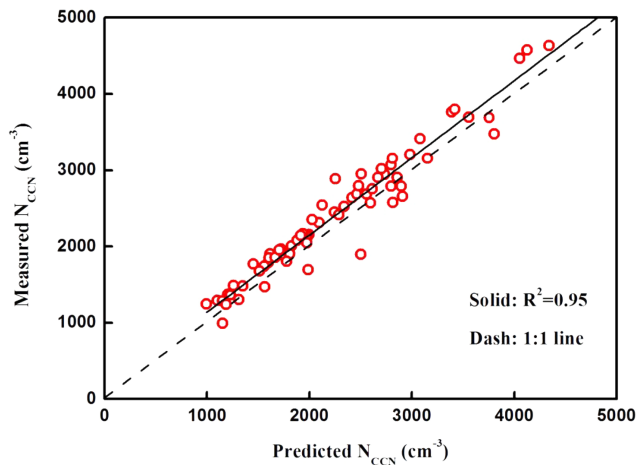
Figure 10. Scatterplot of the simplified closure analysis at SS 0.2 %.

3.3.2 Black carbon and CCN

As a part of hydrophobic aerosols, pure BC particles acquire hydrophilic coatings as they age in the atmosphere, and then the aged BC becomes sufficiently hydrophilic and serves as CCN for cloud condensation formation (Ritesh et al., 2007). On the other hand, BC particles can release sensible heat by effectively absorbing solar radiation, thereby increasing the critical supersaturation of CCN and preventing aerosol to act

as CCN (Conant et al., 2002). Biomass burning emits a large amount of trace gases and carbonaceous particles into the atmosphere, and leads to changes in climate and precipitation, as well as aquatic and terrestrial ecosystem (Andreae et al., 2004). The wild fires contribute a significant fraction of global CCN burden (Pierce et al., 2007; Andreae et al., 2009). Large quantities of active agricultural fire sites were detected from satellites over China on 7 November 2010 (Fig. 1), whereas no obvious wild biomass burning activities were observed during the rest days. Based on the calculated 24 h air mass backward trajectories, the air mass that passed right through the agricultural fire regions in the Jiangsu and Anhui provinces on 7 November reached the sampling site in the next day, bringing large quantities of aged BC particles after a long range transport. This resulted in a severe increase of particle mass concentration and a significant enhancement of aerosol extinction coefficient on 7 and 8 November (Fig. 3). As discussed in Sect. 3.2, NO$_2$ and SO$_2$ concentrations increased synchronously during the whole period (Fig. 6), and they would undergo heterogeneous reactions on the surface of BC particles to change particle microphysical and chemical properties, making BC particles sufficiently hydrophilic to act as CCN (Ritesh et al., 2007).

Relationship analyses between N_{CCN}, N_{CCN}/N_{CN} and BC were calculated using hourly averaged data, and the correlation coefficients (R^2) are presented in Fig. 9. Surprisingly, BC strongly correlated with N_{CCN} ($R^2 = 0.85$) in the foggy–hazy and hazy cases, whereas they showed a poor linear relationship ($R^2 = 0.25$) in the clear case. The possible reason is BC particle aging by heterogeneous reactions with gaseous pollutants (e.g., NO_2 and SO_2) to be activated CCN during pollutant atmospheric transport (Ritesh et al., 2007). In addition, so many studies have proposed that the aged BC is efficient CCN (Dusek. et al., 2006; Anttila and Kerminen, 2007; Hudson, 2007). However, N_{CCN}/N_{CN} was poorly related with BC for both foggy–hazy/hazy and clear cases ($R^2 = 0.43$ and 0.07, respectively), indicating that BC may be a relatively more important contributor to unactivated particles especially in nanoscale sizes (e.g., traffic emission) than activated CCN.

3.4 Relationship of aerosol and CCN

Although aerosol size distributions were measured only in the size range of 10–10 000 nm, they were still used to predict N_{CCN} according to Köhler theory (Köhler et al., 1936). Toward this end, the particle hygroscopicity "kappa" (κ) was used in the closure calculation. The description of the technique has been given by Petters and Kreidenweis (2007); therefore it will only be briefly summarized here. The κ parameter for one multicomponent particle can be obtained through weighting each component κ_i by their volume fractions in the mixture,

$$\kappa = \sum_{i}^{\varepsilon_i \kappa_i}, \tag{1}$$

where ε_i is the volume fraction of chemical compounds in particles, and κ_i is the effective κ of individual chemical composition.

Assuming aerosol particles are completely internally mixed, a simplified κ was calculated using water soluble inorganic ions (organic matter data are unavailable). Aerosol particle compositions were classified into three categories (Petters and Kreidenweis, 2007; Wiedensohler et al., 2009), and κ_i and densities for each component are shown in Table 3, in which "others" is defined as "$PM_{2.5}$-BC-inorganic ions". The critical dry size (CDS) of particle to be activated as CCN at one SS can hence be determined by the following equation:

$$S(D) = \frac{D^3 - D_d^3}{D^3 - D_d^3(1 - \kappa)} \exp\left(\frac{4\sigma_{s/a}M_\omega}{RT\rho_\omega D}\right), \tag{2}$$

where ρ_ω is the density of water, M_ω is the molecular weight of water, $\sigma_{s/a}$ is the surface tension of the solution/air interface, R is the universal gas constant, κ is the hygroscopicity parameter, T is temperature, D_d is the dry diameter, D is the diameter of the droplet and $S(D)$ is the critical dry

size under a given SS. Detailed information for the derivation of Eq. (2) can be found in Petters and Kreidenweis (2007). Equation (2) applies over the entire range of humidity and solution hygroscopicity and can be utilized to predict the conditions of cloud droplet activation. The critical SS for a selected dry size of particle is determined from the maximum of the curve for Eq. (2). Computed for $\sigma_{s/a} = 0.072\,\mathrm{J\,m^{-2}}$ and $T = 298.15\,\mathrm{K}$, the calculated CDS varied between 60 nm and 130 nm and averaged at 102 nm. Particularly, the hourly averaged CDS during the foggy–hazy/hazy cases was slightly lower (96 nm) than during the clear case (105 nm). So far, the comparable or relatively higher CDS has also been found in diverse regions and for various aerosol types, despite different calculation models and SS. For example, the fresh aerosol particles emitted by an aircraft internal combustion engine have a CDS range of 146–301 nm at SS 0.7 %, depending on varying operating conditions (Hitzenberger et al., 2003). Furutani et al. (2008) investigated three types of aerosol masses along the southern coast of California, and the CDS was estimated at 110 nm at SS 0.6 % for fresh ship exhaust, 70–110 nm for fresh anthropogenic aerosols and roughly 50 nm for aged anthropogenic and clean maritime aerosols. In Vienna, the CDS has a wide gap between 69 nm and 368 nm, and averaged at 169 nm (Burkart et al., 2011). Quinn et al. (2008) observed the CDS in a narrow range of 70–90 nm for maritime aerosols in the Gulf of Mexico, and a moderate range of 90–170 nm in the ship channels of Houston with high marine traffic densities close to industrial and anthropogenic sources.

The CCN population can be effectively viewed as a subset of measured aerosol size distributions since the operating range (10–10 000 nm) includes the majority of atmospheric particles. Therefore, the predicted N_{CCN} can be calculated through integrating particles upward in size from the bottom CDS to the upper boundary. In this calculation, the predicted N_{CCN} of hourly averaged CDS was compared with the measured one correspondingly.

The results of this closure analysis are shown in scatterplot in Figs. 10 and 11. The prediction for CCN is generally success throughout the entire data set. The linear regression between predicted and measured N_{CCN} produces a slope of 1.012 and an intercept of 128.3 cm^{-3} ($R^2 = 0.95$), and the average ratio of predicted versus measured N_{CCN} is 0.94 (Fig. 10). The results indicate some moderate underestimate (about 6 % on average) but the agreement is still excellent. The achieved closure calculation suggested that water soluble inorganic ions played a major role in contributing the κ value. In fact, 83.8 % of the κ was expressed by $SO_4^{2-} + NO_3^- + NH_4^+$ in total (in another study by our group, not published yet), with their individual contribution to be 39.8 %, 31.7 % and 12.3 %, respectively. In addition, it is noteworthy that the predicted N_{CCN} at SS 0.2 % was more correlated with the observed N_{CCN} in the clear case ($R^2 = 0.96$) than the foggy–hazy/hazy cases ($R^2 = 0.91$), and the corresponding ratios of predicted to observed N_{CCN} were

0.95 and 0.92, respectively (Fig. 11). In all cases, the mean ratio of predicted to observed N_{CCN} never reached up to 1, suggesting that organic matter would play a second role and make up the rest of κ.

4   Conclusions and discussion

A continuous 4-day data set obtained at an urban site in Shanghai over a fog–haze event from 6 to 9 November 2012 was analyzed for CCN and aerosol. Overall, meteorological conditions such as wind speed, wind direction and temperature exerted a great influence on $PM_{2.5}$ and BC loadings. Human activity is an essential factor to control emissions of aerosol and CCN in urban environments. N_{CCN}/N_{CN} and N_{CCN} usually were higher in the hazy case due to increased aerosols in the accumulation mode, and lower in the foggy–hazy and clear cases. DeFelice et al. (1996) also found the reduction of CCN concentration under foggy and rainy conditions in the Antarctic area. Of special interest, the low N_{CCN}/N_{CN}, N_{CN} and N_{CCN} during the foggy–hazy case can plausibly explain in three aspects: (1) the limited data input introduces some uncertainties, (2) the possible physical effects such as boundary layer evolution, transportation and atmospheric dilution are not considered, (3) the plausible emergence of fog droplets and particles leads to the reduction of aerosol number concentration.

BC was correlated well with N_{CCN} in the foggy–hazy and hazy cases, while they were less linked in the clear case. Besides, there were no good agreements between BC and N_{CCN}/N_{CN}, with moderate ($R^2 = 0.43$) and poor ($R^2 = 0.07$) correlation coefficients for the foggy–hazy/hazy cases and clear case, respectively. More BC is aged during the foggy–hazy/hazy cases; hence more CCN is activated (Dusek et al., 2006; Anttila and Kerminen., 2007; Hudson., 2007). However, a different perspective exists. For example, BC has been found to significantly suppress cloud formation in the Indo–Gangetic plain (Ritesh et al., 2007). Pure BC particles are hydrophobic and can release heat by absorbing solar radiation; hence they would increase the critical SS of aerosol to act as CCN and further suppress the tendency of CCN to become cloud droplets. However, aged BC particles are sufficiently hydrophilic by acquiring hydrophilic coatings in the atmosphere, and become CCN and favor aerosol indirect forcing (Conant et al., 2002; Ritesh et al., 2007). In this study, BC particles moved a long-distance from inland and aged during the transporting process, thereby it favors CCN formation.

By using a simplified κ parameter, the critical dry size never exceeded 130 nm. In spite of the absence of organic matter, the CCN closure calculation was still achieved, suggesting that aerosol major water soluble ions contribute to effective κ. The predicted N_{CCN} was close to the observed during the clear case than the foggy–hazy/hazy cases having more organic matter. In summary, water soluble inorganic ions constituted the majority of particle hygroscopicity (κ) estimation, while organic matter made up the rest. It is noted that organic matter is essential to build the exact CCN prediction models.

This paper mainly explored how N_{CCN}, N_{CN} and N_{CCN}/N_{CN} vary under a fog–haze co-occurring condition, as well as the major influential factors to these activities. The results revealed that the particulate pollutant burden exerts a significant impact on N_{CCN}, especially N_{CCN}/N_{CN} is effectively promoted during the polluted periods (e.g., haze). Importantly, the fog–haze transformation is highly complicated and involves numerous changes of aerosol in physical and chemical properties, which remains poorly understood. The clear and hazy cases both continued more than one day with a reduced effect of diurnal variation. Foggy conditions mostly occur at night and in the morning and seldom last as long as 24 h in Shanghai; therefore it was inevitable that the diurnal variations had some effect on the results during the foggy–hazy case spanning from 23:00 LT on 6 November to 10:00 LT on 7 November. This represents the results of only one case, and more efforts are needed to highlight the comprehensive effects of fog and haze on CCN in urban environments.

References

Andreae, M. O.: Correlation between cloud condensation nuclei concentration and aerosol optical thickness in remote and polluted regions, Atmos. Chem. Phys., 9, 543–556, doi:10.5194/acp-9-543-2009, 2009.

Andreae, M. O., Rosenfeld, D., Artaxo, P., Costa, A. A., Frank, C. P., Longo, K. M., and Silva-Dias, M. A. F.: Smoking rain clouds over the Amazon, Science, 303, 1337–1342, doi:10.1126/science.1092779, 2004.

Andreae, M. O., Jones, C. D., and Cox. P. M.: Strong present-day aerosol cooling implies a hot future, Nature, 435, 1187–1190, 2005.

Anttila, T. and Kerminen, V.-M.: On the contribution of Aitken mode particles to cloud droplet populations at continental back-

ground areas – a parametric sensitivity study, Atmos. Chem. Phys., 7, 4625–4637, doi:10.5194/acp-7-4625-2007, 2007.

Baumgardner, D., Raga, G. B., and Muhlia, A.: Evidence for the formation of CCN by photochemical processes in Mexico City, Atmos. Environ., 38, 357–367, doi:10.1016/j.atmossenv.2003.10.008, 2003.

Biswas, K. F., Ghauri, B. M., and Husain, L.: Gaseous and aerosol pollutants during fog and clear episodes in South Asian urban atmosphere, Atmos. Environ., 42, 7775–7785, 2008.

Boers, R., and Eloranta, E.W.: Lidar measurements of the atmospheric entrainment zone and the potential temperature jump across the top of the mixed layer, Bound.-Lay. Meteorol., 34, 357–375, 1986.

Brooks, I. M.: Finding boundary layer top: application of a wavelet covariance transform to lidar backscatter profiles, J. Atmos. Ocean. Tech., 20, 1092–1105, 2003.

Burkar, J., Steiner, G., Reischl, G., and Hitzenberger, R.: Long-term study of cloud condensation nuclei (CCN) activation of atmospheric aerosol in Vienna, Atmos. Environ., 45, 5751–5759, 2011.

Campbell, J. R., Hlavka, D. L., Welton, E. J., Flynn, C. J., Turner, D. D., Spinhirne, J. D., Scott, V. S., and Hwang, I. H.: Full-time, eye-safe cloud and aerosol lidar observation at atmospheric radiation measurement program sites: Instruments and data processing, J. Atmos. Ocean. Technol., 19, 431–442, 2002.

Che, H. Z., Zhang, X. Y., Li, Y., Zhou, Z. J., Qu, John. J and Hao, X. J.: Haze trends over the capital cities of 31 provinces in China, 1981–2005, Theor. Appl. Climatol., 97, 235–242, 2009.

Cheng, T. T., Han, Z. W., Zhang, R. J., Du, H. H., Jia, X., Wang, J. J., and Yao, J. Y.: Black carbon in a continental semi-arid area of Northeast China and its possible sources of fire emission, J. Geophys. Res., 115, D23204, doi:10.1029/2009JD013523, 2010.

Cheng, Y., Lee, S. C., Ho, K. F., Wang, Y. Q., Cao, J. J., Chow, J. C., and Watson, J. G.: Black carbon measurement in a coastal area of south China, J. Geophys. Res., 111, D12310, doi:10.1029/2005JD006663, 2006.

Cohn, S. A., Angevine, W. M.: Boundary layer height and entrainment zone thickness measured by lidars and wind-profiling radars, J. Appl. Meteorol., 39, 1233–1247, 2000.

Conant, W. C., A. Netes, and J. H. Seinfeld.: Black carbon radiative heating effectson cloud microphysics and implications for the aerosol indirect effect: 1. Extented Köhler theory, J. Geophys. Res., 107, 4604, doi:10.1029/2002JD002094, 2002.

Cubison, M. J., Ervens, B., Feingold, G., Docherty, K. S., Ulbrich, I. M., Shields, L., Prather, K., Hering, S., and Jimenez, J. L.: The influence of chemical composition and mixing state of Los Angeles urban aerosol on CCN number and cloud properties, Atmos. Chem. Phys., 8, 5649–5667, doi:10.5194/acp-8-5649-2008, 2008.

DeFelice, T. P.: Variation in cloud condensation nuclei at palmer station Antarctica during February 1994, Atmos. Res., 41, 229–248, 1996.

Deng, Z. Z., Zhao, C. S., Ma, N., Liu, P. F., Ran, L., Xu, W. Y., Chen, J., Liang, Z., Liang, S., Huang, M. Y., Ma, X. C., Zhang, Q., Quan, J. N., Yan, P., Henning, S., Mildenberger, K., Sommerhage, E., Schäfer, M., Stratmann, F., and Wiedensohler, A.: Size-resolved and bulk activation properties of aerosols in the North China Plain, Atmos. Chem. Phys., 11, 3835–3846, doi:10.5194/acp-11-3835-2011, 2011.

Draxler, R. R. and Rolph, G. D.: HYSPLIT (Hybrid Single-Particle Lagrangian Integrated Trajectory) Model access via NOAA ARL READY Website (http://www.arl.noaa.gov/ready/hysplit4.htm), NOAA Air Resources Laboratory, Silver Spring, MD, 2003.

Du, H. H., Kong, L. D., Cheng, T. T., Chen, J. M., Du, J. F., Li, L., Xia, X., Leng, C. P., and Huang, G. H.: Insights into summertime haze pollution events over Shanghai based on online water-soluble ionic composition of aerosols, Atmos. Environ., 45, 5131–5137, 2011.

Dumka, U. C., Krishna Moorthy, K., Kumar, R., Hegde, P., Sagar, R., Pant, P., Singh, N., and Suresh Babu, S.: Characteristics of aerosol black carbon mass concentration over a high altitude location in the Central Himalayas from multi-year measurements, Atmos. Res., 96, 510–521, 2010.

Dusek, U., Frank, G. P., and Hildebrandt, L.: Size matters more than chemistry for cloud-nucleating ability of aerosol particles, Science, 312, 1375–1378, 2006.

Elizabeth, R. G., Paula, K. H., and Vicki, H. G.: Physicochemical properties of nitrate aerosols: implications for the atmosphere, J. Phys. Chem., 110, 11785–11799, 2006.

Ferin, J., Oberdoerster, G., Penney, D. P., Soderholm, S. C., Gelein, R., and Piper, H. C.: Increased pulmonary toxicity of ultrafine particles 1. Particles clearance, translocation, morphology, J. Aerosol Sci., 21, 381–384, 1990.

Fernald, F. G.: Analysis of atmospheric lidar observations: Some comments, Appl. Opt., 23, 652–653, 1984.

Fisak, J., Tesar, M., Rezacova, D., Elias, V., Weignerova, V., and Fottova, D.: Pollutant concentrations in fog and low cloud water at selected sites of the Czech Republic, Atmos. Res., 64, 75–87, 2002. Fu, Q. Y., Zhuang, G. S., Wang, J., Xu, C., Huang, K., Li, J., Hou, B., Lu,

Fu, Q. Y., Zhuang, G. S., Wang, J., Xu, C., Huang, K., Li, J., Hou, B., Lu, T., and Streets, D. G.: Mechanism of formation of the heaviest pollution episode ever recorded in the Yangtze River Delta, China, Atmos. Environ., 42, 2023–2036, 2008.

Furutani. H., Dall'Osto, M., Roberts, G. C., and Prather, K. A.: Assessment of the relative importance of atmospheric aging on CCN activity derived from field observations, Atmos. Environ., 42, 3130–3142, 2008.

Gao, J., Wang, T., Zhou, X. H., Wu, W. S., and Wang, W. X.: Measurement of aerosol number size distributions in the Yangtze River delta in China: formation and growth of particles under polluted conditions, Atmos. Environ., 43, 829–836, 2009.

Gautam, R., Hsu, N. C., Kafatos, M., and Tsay, S. C.: Influences of winter haze on fog/low cloud over the Indo-Gangetic plains, J. Geophys. Res., 112, D05207, doi:10.1029/2005JD007036, 2007.

Gulpete, I., Tardif, R., Michaelides, S. C., Cermak, J., Bott, A., Bendix, J., Müller, M. D., Pagowski, M., Hansen, B., Ellrod, G., Jacobs, W., Toth, G., and Cober, S. G.: Fog research: a review of past achievements and future perspectives, Pure Appl. Geophys., 164, 1121–1159, 2007.

Hagler, G. S. W., Bergin, M. H., Smith, E. A., and Dibb, J. E.: A summer time series of particulate carbon in the air and snow at Summit, Greenland, J. Geophys. Res., 112, D21309, doi:10.1029/2007JD008993, 2007.

Hansen, A. D. A., Rosen, H., and Novakov, T.: The aethalometer – an instrument for the real-time measurement of optical absorption by aerosol particles, Sci. Total Environ., 36, 191–196, 1984.

He, Q. S., Li, C. C., Mao, J. T., Lau, A. K. H., and Li, P. R.: A study on the aerosol extinction-to-backscatter ratio with combination of micro-pulse LIDAR and MODIS over Hong Kong, Atmos. Chem. Phys., 6, 3243–3256, doi:10.5194/acp-6-3243-2006, 2006.

Henning, S., Wex, H., Hennig, T., Kiselev, A., Snider, J. R., Rose, D., Dusek, U., Frank, G. P., Pöschl, U., Kristensson, A., Bilde, M., Tillmann, R., Kiendler-Scharr, A., Mentel, T. F., Walter, S., Schneider, J., Wennrich, C., and Stratmann, F.: Soluble mass, hygroscopic growth, and droplet activation of coated soot particles during LACIS Experiment in November (LExNo), J. Geophys. Res., 115, D11206, doi:10.1029/2009JD012626, 2010.

Herckes, P., Chang, H., Lee, T., and Collett Jr., J. L.: Air pollution processing by radiation fogs, Water Air Soil Poll., 181, 65–75, 2007.

Hings, S. S., Wrobel, W. C., Cross, E. S., Worsnop, D. R., Davidovits, P., and Onasch, T. B.: CCN activation experiments with adipic acid: effect of particle phase and adipic acid coatings on soluble and insoluble particles, Atmos. Chem. Phys., 8, 3735–3748, doi:10.5194/acp-8-3735-2008, 2008.

Hitzenberger, R., Giebl, H., Petzold, A., Gysel, M., Nyeki, S., Weingartner, E., Baltensperger, U., and Wilson, W. C.: Properties of jet engine combustor particles during the PartEmis experiment, hygroscopic properties at supersaturated conditions, Geophys. Res. Lett., 30, 1779, doi:10.1029/2003GL017294, 2003.

Hudson, J.: Variability of the relationship between particle size and cloud-nucleating ability, Geophys. Res. Lett., 34, L08801, doi:10.1029/2006GL028850, 2007.

Hudson, J. G. and Noble, S.: CCN and vertical velocity influence on droplet concentration and supersaturations in clean and polluted stratus clouds, J. Atmos. Sci., 106, 24119–24126, 2014. IPCC: Climate Change 2013: The Physical Science Basis. Contribution of Working Group to the Fifth Assessment Report of the Intergovernmental Panel on Climate Change, edited by: Joussaume, S., Penner, J., and Tangang, F., IPCC, Stockholm, 2013.

Jimenez, J. L., Canagaratna, M. R., Donahue, N. M., Prevot, A. S. H., Zhang, Q., Kroll, L. H., DeCarlo, P. F., Allan, J. D., Coe, H., Ng, N. L., Ailen, A. C., Docherty, K. S., Ulbrich, I. M., Grieshop, A. P., Robinson, A. L., Duplissy, J., Smith, J. D., Wilson, K. R., Lanz, V. A., Hueglin, C., Sun, Y. L., Tian, J., Laakonen, A., Raatikainen, T., Rautiainen, J., Vaattovaara, P., Ehn, M., Kulmala, M., Tomlinson, J. M., Collins, D. R., Cubison, M. J., Dunlea, E. J., Huffman, J. A., Onasch, T. B., Alfarra, M. R., Williams, P. I., Bower, K., Kondo, Y., Schneider, J., Drewnick, F., Borrmann, S., Weimer, S., Demerjian, K., Salcedo, D., Cottrell, L., Griffin, R., Takami, A., Miyoshi, T., Hatakeyama, S., Shimono, A., Sun, J. Y., Zhang, Y. M., Dzepina, K., Kimmel, J. R., Sueper, D., Jayne, J. T., Herndon, S. C., Trimborn, A. M., Williams, L. R., Wood, E. C., Middlebrook, A. M., Kolb, C. E., Baltensperger, U., and Worsnop, D. R.: Evolution of organic aerosols in the atmosphere, Science, 326, 1525–1529, 2009.

Jurányi, Z., Gysel, M., Weingartner, E., DeCarlo, P. F., Kammermann, L., and Baltensperger, U.: Measured and modelled cloud condensation nuclei number concentration at the high alpine site Jungfraujoch, Atmos. Chem. Phys., 10, 7891–7906, doi:10.5194/acp-10-7891-2010, 2010.

Köhler, H.: The nucleus in and the the growth of hygroscopic droplets, T. Faraday Soc., 32, 1152–1161, 1936.

Kuang, C., McMurry, P. H., and McCormick, A. V.: Determination of cloud condensation nuclei production from measured new particle formation events, Geophys. Res. Lett., 36, L09822, doi:10.1029/2009GL037584, 2009.

Kuwata, M. and Kondo, Y.: Dependence of size-resolved CCN spectra on the mixing state of nonvolatile cores observed in Tokyo, J. Geophys. Res., 113, D19202, doi:10.1029/2007JD009761, 2008.

Kuwata, M., Kondo, Y., Mochida, M., Takegawa, N., and Kawamura, K.: Dependence of CCN activity of less volatile particles on the amount of coating observed in Tokyo, J. Geophys. Res., 112, D11207, doi:10.1029/2006JD007758, 2007.

Lance, S., Medina, J., Smith, J. N., and Nenes, A.: Mapping the operation of the DMT Continuous Flow CCN counter, Aerosol Sci. Tech., 40, 242–254, 2006.

Lathem, T. L. and Nenes, A.: Water vapor depletion in the DMT Continuous Flow CCN Chamber: effects on supersaturation and droplet growth, Aerosol Sci. Tech., 45, 604–615, 2011.

Leng, C. P., Cheng, T. T., Chen, J. M., Zhang, R. J., Tao, J., Huang, G. H., Zha, S. P., Zhang, M. G., Fang, W., Li, X., and Li, L.: Measssurements of surface cloud condensation nuclei and aerosol activity in downtown Shanghai, Atmos. Environ., 69, 354–361, 2013.

Liu, J. J., Zheng, Y. F., Li, Z. Q., and Cribb, M.: Analysis of cloud condensation nuclei properties at a polluted site in southeastern China during the AMF-China Campaign, J. Geophys. Res., 116, D00K35, doi:10.1029/2011JD016395, 2011.

Lohmann, U. and Feichter, J.: Global indirect aerosol effects: a review, Atmos. Chem. Phys., 5, 715–737, doi:10.5194/acp-5-715-2005, 2005.

Matsui, H., Koike, M., Kondo, Y., Takegawa, N., Fast, J. D., Pöschl, U., Garland, R. M., Andreae, M. O., Wiedensohler, A., Sugimoto, N., and Zhu, T.: Spatial and temporal variations of aerosols around Beijing in summer 2006: 2. Local and column aerosol optical properties, J. Geophys. Res., 115, D22207, doi:10.1029/2010JD013895, 2010.

Menut, L., Flamant, C., Pelon, J., and Flamant, P. H.: Urban boundary-layer height determination from lidar measurements over the Paris area, Appl. Optics, 38, 945–954, 1999.

Merikanto, J., Spracklen, D. V., Mann, G. W., Pickering, S. J., and Carslaw, K. S.: Impact of nucleation on global CCN, Atmos. Chem. Phys., 9, 8601–8616, doi:10.5194/acp-9-8601-2009, 2009.

Moffet, R. C., de Foy, B., Molina, L. T., Molina, M. J., and Prather, K. A.: Measurement of ambient aerosols in northern Mexico City by single particle mass spectrometry, Atmos. Chem. Phys., 8, 4499–4516, doi:10.5194/acp-8-4499-2008, 2008.

Petters, M. D. and Kreidenweis, S. M.: A single parameter representation of hygroscopic growth and cloud condensation nucleus activity, Atmos. Chem. Phys., 7, 1961–1971, doi:10.5194/acp-7-1961-2007, 2007.

Petzold, A., Kopp, C., and Niessner, R.: The dependence of the specific attenuation cross-section on black carbon mass fraction and particle size, Atmos. Environ., 31, 661–672, 1997.

Pierce, J. R., Chen, K., and Adams, P. J.: Contribution of primary carbonaceous aerosol to cloud condensation nuclei: processes and uncertainties evaluated with a global aerosol microphysics model, Atmos. Chem. Phys., 7, 5447–5466, doi:10.5194/acp-7-5447-2007, 2007.

Qian, Y., Kaiser, D. P., Leung, L. R., and Xu, M.: More frequent cloud-free sky and less surface solar radiation in China from 1955–2000, Geophys. Res. Lett., 33, L01812, doi:10.1029/2005GL024586, 2006.

Quinn, P. K., Bates, T. S., Coffman, D. J., and Covert, D. S.: Influence of particle size and chemistry on the cloud nucleating properties of aerosols, Atmos. Chem. Phys., 8, 1029–1042, doi:10.5194/acp-8-1029-2008, 2008.

Reade, L., Jennings, S. G., and Gobnait, M.: Cloud condensation nuclei measurements at Mace Head, Ireland, over the period 1994–2002, Atmos. Res., 82, 610–621, 2006.

Ritesh, G., Christina, H., Menas. Kafatos., Si-Chee. T.: Influences of winter haze on fog/low cloud over the Indo-Gangetic plains, J. Geophys. Res., 112, D05207, doi:10.1029/2005JD007036, 2007.

Roberts, G. C. and Nenes, A.: A continuous-flow streamwise thermal-gradient CCN chamber for atmospheric measurements, Aerosol Sci. Tech., 39, 206–221, 2005.

Rose, D., Nowak, A., Achtert, P., Wiedensohler, A., Hu, M., Shao, M., Zhang, Y., Andreae, M. O., and Pöschl, U.: Cloud condensation nuclei in polluted air and biomass burning smoke near the mega-city Guangzhou, China – Part 1: Size-resolved measurements and implications for the modeling of aerosol particle hygroscopicity and CCN activity, Atmos. Chem. Phys., 10, 3365–3383, doi:10.5194/acp-10-3365-2010, 2010.

Rose, D., Gunthe, S. S., Su, H., Garland, R. M., Yang, H., Berghof, M., Cheng, Y. F., Wehner, B., Achtert, P., Nowak, A., Wiedensohler, A., Takegawa, N., Kondo, Y., Hu, M., Zhang, Y., Andreae, M. O., and Pöschl, U.: Cloud condensation nuclei in polluted air and biomass burning smoke near the mega-city Guangzhou, China – Part 2: Size-resolved aerosol chemical composition, diurnal cycles, and externally mixed weakly CCN-active soot particles, Atmos. Chem. Phys., 11, 2817–2836, doi:10.5194/acp-11-2817-2011, 2011.

Rosenfeld, D., Dai, J., Yu, X., Yao, Z., Xu, X., Wang, X., and Du, C.: Inverse relations between amounts of air pollution and orographic precipitation, Science, 315, 1396–1398, 2007.

Rosenfeld, D., Lohmann, U., Raga, G. B., O'Dowd, C. D., Kulmala, M., Fuzzi, S., Reissell, A., and Andreae, M. O.: Flood or drought: how do aerosol affects precipitation?, Science, 321, 1309–1313, 2008.

Shao, M., Tang, X., Zhang, Y., and Li, W.: City clusters in China: air and surface water pollution, Front. Ecol. Environ., 4, 353–361, 2006.

Sihto, S.-L., Mikkilä, J., Vanhanen, J., Ehn, M., Liao, L., Lehtipalo, K., Aalto, P. P., Duplissy, J., Petäjä, T., Kerminen, V.-M., Boy, M., and Kulmala, M.: Seasonal variation of CCN concentrations and aerosol activation properties in boreal forest, Atmos. Chem. Phys., 11, 13269–13285, doi:10.5194/acp-11-13269-2011, 2011.

Stone, E. A., Snyder, D. C., Sheesley, R. J., Sullivan, A. P., Weber, R. J., and Schauer, J. J.: Source apportionment of fine organic aerosol in Mexico City during the MILAGRO experiment 2006, Atmos. Chem. Phys., 8, 1249–1259, doi:10.5194/acp-8-1249-2008, 2008.

Streets, D. G., Tsia, N. Y., Akimoto, H., and Oka, K.: Sulfur dioxide emissions in Asia in the period 1985–1997, Atmos. Environ., 34, 4413–4424, 2000.

Streets, D. G., Yu, C., Wu, Y., Chin, M., Zhao, Z., Hayasaka, T., and Shi, G.: Aerosol trends over China, 1980–2000, Atmos. Res., 88, 174–182, 2008.

Sun, Y. L., Zhuang, G. S., Tang, A. H., Wang, Y., and An, Z. S.: Chemical characteristics of $PM_{2.5}$ in haze-fog episodes in Beijing, Environ. Sci. Technol., 40, 3148–3155, 2006.

Svenningsson, B., Rissler, J., Swietlicki, E., Mircea, M., Bilde, M., Facchini, M. C., Decesari, S., Fuzzi, S., Zhou, J., Mønster, J., and Rosenørn, T.: Hygroscopic growth and critical supersaturations for mixed aerosol particles of inorganic and organic compounds of atmospheric relevance, Atmos. Chem. Phys., 6, 1937–1952, doi:10.5194/acp-6-1937-2006, 2006.

Tie, X. and Cao, J.: Aerosol pollution in China: present and future impact on environment, Particuology., 7, 426–443, 2009.

Urone, P., Lutsep, Helmut., Noyes. C. M., and Parcher, J. F.: Static studies of sulfur dioxide reactions in air, Environ. Sci. Technol., 2, 611–618, 1968.

Wang, Y., Zhuang, G. S., Zhang, X. Y., Huang, K., Xu, C., Tang, A. H., Chen, J. M., and An, Z. S.: The ion chemistry, seasonal cycle, and sources of $PM_{2.5}$ TSP aerosol in Shanghai, Atmos. Environ., 40, 2935–2952, 2006.

Weingartner, E., Saathoff, H., Schnaiter, M., Streit, N., Bitnar, B., and Baltensperger, U.: Absorption of light by soot particles: determination of the absorption coefficient by means of aethalometers, J. Aerosol Sci., 34, 1445–1463, 2003.

Wiedensohler, A., Cheng, Y. F., Nowak, A., Wehner, B., Achtert, P., Berghof, M., Birmili, W., Wu, Z. J., Hu, M., Zhu, T., Takegawa, N., Kita, K., Kondo, Y., Lou, S. R., Hofzumahaus, A., Holland, F., Wahner, A., Gunthe, S. S., Rose, D., Su, H., and Pöschl, U.: Rapid aerosol growth and increase of cloud condensation nucleus activity by secondary aerosol formation and condensation: a case study for regional air pollution in northeastern China, Geophys. Res. Lett., 114, D00G08, doi:10.1029/2008JD010884, 2009.

Ye, X. N., Ma, Z., Zhang, J. C., Du, H. H., Chen, J. M., Chen, H., Yang, X., Gao, W., and Geng, F. H.: Important role of ammonia on haze formation in Shanghai, Environ. Lett., 6, 024019, doi:10.1088/1748-9326/6/2/024019, 2011.

Yu, F., Wang, Z., Luo, G., and Turco, R.: Ion-mediated nucleation as an important global source of tropospheric aerosols, Atmos. Chem. Phys., 8, 2537–2554, doi:10.5194/acp-8-2537-2008, 2008.

Yue, D. L., Hu, M., Zhang, R. J., Wu, Z. J., Su, H., Wang, Z. B., Peng, J. F., He, L. Y., Huang, X. F., Gong, Y. G., and Wiedensohler, A.: Potential contribution of new particle formation to cloud condensation nuclei in Beijing, Atmos. Environ., 45, 6070–6077, 2011.

Yum, S. S. and James, G. H.: Wintertime/summertime contrasts of cloud condensation nuclei and cloud microphysics over the South Ocean, J. Geophys. Res., 109, D06204, doi:10.1029/2003JD003864, 2004.

Yum, S. S., James, G. H, Keun, Y. S., and Byoung-Cheol, C.: Springtime cloud condensation nuclei concentrations on the west coast of Korea, Geophys. Res. Lett., 32, L09814, doi:10.1029/2005GL022641, 2005.

Zhang, M., Wang, X. M., Chen, J. M., Cheng, T. T., Wang, T., Yang, X., Gong, Y. G., Geng, F. H., and Chen, C. H.: Physical characterization of aerosol particles during the Chinese New Year's firework events, Atmos. Environ., 44, 5191–5198, 2010.

Zhang, Q., Tie, X. X., Lin, W. L., Cao, J. J., Quan, J. N., Ran, L., and Xu, W. Y.: Variability of SO$_2$ in an intensive fog in North China Plain: evidence of high solubility of SO$_2$, Particuology, 11, 41–47, 2013.

Zhang, R., Jing, J., Tao, J., Hsu, S.-C., Wang, G., Cao, J., Lee, C. S. L., Zhu, L., Chen, Z., Zhao, Y., and Shen, Z.: Chemical characterization and source apportionment of PM$_{2.5}$ in Beijing: seasonal perspective, Atmos. Chem. Phys., 13, 7053–7074, doi:10.5194/acp-13-7053-2013, 2013.

Zhang, X. Y., Zhuang, G. S., Chen, J. M., Wang, Y. X., An, Z. S., Zhang, P.: Heterogeneous reactions of sulfur dioxide on typical mineral particles, J. Phys. Chem. B, 110, 12588–12596, 2006.